

Discoveries of 3 K-shell Lines of Iron and a Coherent Pulsation of 593-sec from SAX J1748.2–2808

Masayoshi NOBUKAWA, Katsuji KOYAMA, Hironori MATSUMOTO, and Takeshi Go TSURU
Department of Physics, Graduate school of Science, Kyoto University, Sakyo-ku, Kyoto 606-8502
nobukawa@cr.scphys.kyoto-u.ac.jp, koyama@cr.scphys.kyoto-u.ac.jp

(Received 2008 May 19; accepted)

Abstract

SAX J1748.2–2808 is a unique X-ray object with a flat spectrum and strong emission lines at 6.4–6.7 keV. The Suzaku satellite resolved the emission lines into 3 K-shell lines from neutral and highly ionized irons. A clear coherent pulsation with a period of 593-sec was found from the Suzaku and XMM-Newton archives. These facts favor that SAX J1748.2–2808 is an intermediate polar, a subclass of magnetized white dwarf binary (cataclysmic variable: CV). This paper reports on details of the findings and discusses the origin of this source.

Key words: Galaxy: Center—Magnetic Cataclysmic Variable —Intermediate Polar — X-ray spectra

1. Introduction

SAX J1748.2–2808 was discovered with the Beppo-SAX satellite in the direction of the giant molecular cloud Sgr D (Sidoli et al. 2001), and was deeply re-observed with the XMM-Newton satellite (Sidoli et al. 2006). The X-ray spectrum was well-fitted with a power-law of index 1.4 plus a broad line of 0.43 keV (1σ) with the center energy at 6.6 keV. The N_{H} value was as large as 1.4×10^{23} H cm $^{-2}$ (Sidoli et al. 2006). SAX J1748.2–2808 was thus regarded as one of the brightest samples of resolved point sources in the Galactic center region (GC) with Chandra deep-exposure observations (Muno et al. 2003, Muno et al. 2006). The integrated spectra of the point sources resemble the Galactic center diffuse X-rays (GCDX) in the iron line features close to 6.4–6.7 keV (Muno et al. 2004, Koyama et al. 2007b). Therefore, these, including SAX J1748.2–2808, can be regarded as significantly contributing to the GCDX, even though SAX J1748.2–2808 was brighter than most of the other point sources in the GC.

The XMM-Newton spectrum favored that SAX J1748.2–2808 is a High Mass X-ray Binary (HMXB) pulsar located at the GC region (Sidoli et al. 2006). However, no coherent pulsation was reported from either the Beppo-SAX or the XMM-Newton observations. Furthermore, the broad line of 0.43 keV (1σ) is very unusual as a HMXB. If this broadening is due to the Doppler effect, the velocity dispersion is as large as 2×10^4 km s $^{-1}$. No such HMXB has been reported so far (e.g. Nagase 1989). The detailed spectrum of SAX J1748.2–2808 did not indicate whether the spectral nature is thermal or non-thermal.

In order to solve the nature of this unique object, we analyzed the Suzaku data of two pointing observations on supernova remnants (SNR), Sgr D SNR and G 0.9+0.1, and also re-analyzed the XMM-Newton archive data.

2. Observations and Data Reduction

The Suzaku and XMM-Newton observations of SAX J1748.2–2808 are listed in table 1. The Suzaku satellite observed two SNRs, Sgr D SNR and G 0.9+0.1, where SAX J1748.2–2808 was located near to the field edge of the XIS CCD Cameras. XIS consists of four sets of X-ray CCD camera systems (XIS 0, 1, 2, and 3) placed on the focal planes of four X-Ray Telescopes (XRT) aboard the Suzaku satellite. XIS 0, 2, and 3 have front-illuminated (FI) CCDs, while XIS 1 has a back-illuminated (BI) CCD. One of the FI CCD cameras (XIS 2) has been out of function since September, 2006, and hence we did not use it. Detailed descriptions of the Suzaku satellite, XRT, and XIS can be found in Mitsuda et al. (2007), Serlemitsos et al. (2007), and Koyama et al. (2007a).

The XIS observations were made with the normal mode. The XIS pulse-height data for each X-ray event were converted to Pulse Invariant (PI) channels using the `xispi` software version 2007-03, and the calibration database version 2008-01-31. We removed the data during the epoch of low-Earth elevation angles less than 5 degrees ($\text{ELV} < 5^\circ$), day Earth elevation angles less than 10 degrees ($\text{DYE_ELV} < 10^\circ$), and the South Atlantic Anomaly. The good exposure times are listed in table 1. Although the XIS CCDs were significantly degraded by on-orbit particle radiation, the CCD performances were restored by the SCI technique (Uchiyama et al. 2008). Then, the overall spectral resolutions (FWHM) at 5.9 keV were ~ 150 and ~ 170 eV for the FI and BI CCDs, respectively. We analyzed the data using the software package HEASoft 6.4.1. For the spectral fittings, we made XIS response files using `xisrmfgen`, and auxiliary files using `xissimarfgen`. Since the spectrum of the non-X-ray background (NXB) depends on the geomagnetic cut-off rigidity (COR) (Tawa et al. 2008), we obtained COR-sorted NXB spectra using `xisnxbgen`, from the night-Earth data released by the Suzaku XIS team.

Table 1. Observation data list

Observatory/Instrument	Target	Obs. ID	Date (yyyy/mm/dd)	Good Exposure Time* (ksec)
Suzaku/XIS	Sgr D SNR	502020010	2007/09/06	139.1
Suzaku/XIS	G 0.9+0.1	502051010	2008/03/11	138.8
XMM-Newton/MOS	Sgr D SNR	0112970101	2000/09/23	15.7
XMM-Newton/PN	Sgr D SNR	0112970101	2000/09/23	11.5
XMM-Newton/MOS	G 0.9+0.1	0144220101	2003/03/12	49.5
XMM-Newton/MOS	SAX J1748.2-2808	0205240101	2005/02/26	50.2
XMM-Newton/PN	SAX J1748.2-2808	0205240101	2005/02/26	41.5

* After the data screening described in the text.

SAX J1748.2–2808 was also in the field of view of the XMM-Newton observations on Sgr D SNR and G 0.9+0.1 on September 2000 and March 2003, respectively. The pointing observation on SAX J1748.2–2808 was also made on February, 2005. The X-ray data were obtained with the European Photon Imaging Camera (EPIC) (Strüder et al. 2001; Turner et al. 2001) cameras in an extended full-frame mode. The data were analyzed using the Science Analysis Software (SAS 7.1.0). Event files for both the PN and the Metal Oxide Semiconductor (MOS) detectors were produced using the `epchain` and `emchain` tasks of SAS, respectively. The event files were screened for high particle-background periods. Good exposure times are listed in table 1. In our analysis, we used the events corresponding to patterns 0–4 for the PN and 0–12 for the MOS instruments. The PN data of SAX J1748.2–2808 on the 2003 observation were not available.

3. Analysis and Results

3.1. X-ray Image

The X-ray images in the Suzaku observations were separately analyzed. Since the Suzaku nominal position error is $\sim 30''$, we fine-tuned the Suzaku position while refereeing to the positions of XMM-Newton sources. In the Sgr D SNR observation, we found an XMM-Newton source S10 (see table 4 of Sidoli et al. 2006). The XMM-Newton position of S10 is $(\alpha, \delta) = (267^\circ 24531, -28^\circ 188918)$, while the Suzaku position is $(\alpha, \delta) = (267^\circ 24409, -28^\circ 185869)$. We therefore shifted the Suzaku coordinate by $(\Delta\alpha, \Delta\delta) = (0^\circ 00122, -0^\circ 003049)$. In the G0.9+0.1 observation, we used an XMM source S2 (see table 4 of Sidoli et al. 2006). The XMM Newton position is $(\alpha, \delta) = (266^\circ 81562, -28^\circ 181511)$, while the Suzaku position is $(\alpha, \delta) = (266^\circ 81737, -28^\circ 180065)$. We hence shifted the Suzaku coordinate by $(\Delta\alpha, \Delta\delta) = (-0^\circ 00175, -0^\circ 001446)$. After these fine-tunings of the Suzaku coordinate, we made the X-ray map shown in figure 1. We found two sources near to the edge of each field. These two sources coincide in position with SAX J1748.2–2808 (strong source) and S12 (faint source) of the XMM-Newton observation within statistical errors of $\leq 5''$.

In order to estimate the intensity ratio of the two sources, we made a projected profile along the line con-

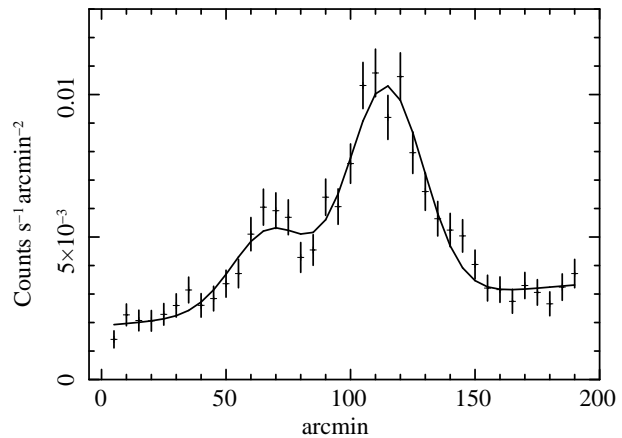


Fig. 2. Projected profile along the line connecting SAX J1748.2–2808 and the faint source (S12). This profile was made from the data in the dashed rectangle in figure 1a and 1b and add together. The solid lines are the best-fit liner function and 2-Gaussians.

necting SAX J1748.2–2808 and the faint source (S12) (see figure 1c). The profile was fitted with two Gaussians plus a liner function, as is shown in figure 2. The widths ($1\text{-}\sigma$) of the Gaussians approximate the projected point-spread function. The best-fit source fluxes (normalizations of the Gaussians) were determined to be 7.5×10^{-3} and 2.8×10^{-3} counts s^{-1} , for SAX J1748.2–2808 and for the faint source (S12), respectively.

3.2. Spectrum

Since the X-ray spectrum of XMM-Newton has already been reported, we obtained the Suzaku spectrum of SAX J1748.2–2808. The point-spread function of XRT has a complicated polygon shape images, due together to the 4-segments structure of the XRT and image deformation near the field edge (Serlemitsos et al. 2007). We therefore extracted the spectra from the solid polygons in figures 1a and 1b, for the best S/N ratio within limited statistics. The background spectra were obtained from a near-by sky shown by the dashed squares, from which the dashed elliptical regions were excluded. For both the source and the background data, we made COR distributions and composed the non-X-ray background (NXB) spectra from the COR-sorted NXB data set (see section

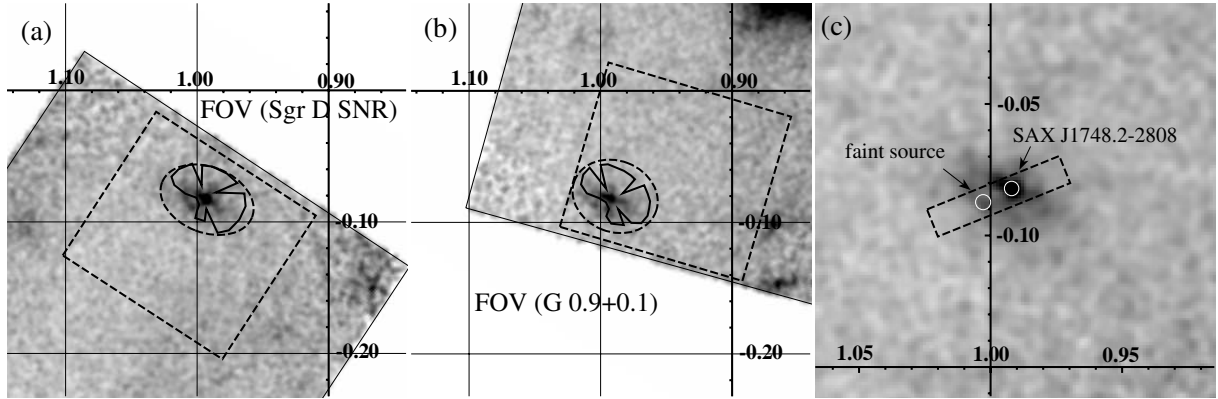


Fig. 1. X-ray map in the 3–7 keV band from the Suzaku observations on Sgr D SNR (a) and G 0.9+0.1 (b). The source regions of SAX J1748.2–2808 are given by the solid polygons, which trace the complicated point-spread function of XRT in the field edge (see text). The dashed squares (excluding ellipses) are the local backgrounds. (c): Combined images of figures (a) and (b) near SAX J1748.2–2808. The projected profile (figure 2) was made from the dashed rectangle region, where the white circles indicate the positions of SAX J1748.2–2808 (strong source) and S12 (faint source) (Sidoli et al. 2006).

2). We then subtracted the NXB from the same detector areas. After NXB subtraction, we corrected the difference in the effective area due to the different off-axis angles between the source and the background regions (Hyodo et al. 2008), and further subtracted the local background (the Cosmic X-ray background plus the Galactic center diffuse X-rays near the source) from the source spectra. The source spectra in the two observations and those of 2 FIs (XIS 0 and XIS 3) were co-added to increase the statistics. We estimated the contamination of the near-by faint source S12 by a ray-tracing simulation (*xissim* in the HEASoft package) using the flux ratio determined in section 3-1, and found that the contamination was $\leq 10\%$ in the energy range 3–10 keV. We therefore ignore the contamination of S12 in the following analysis and discussion.

The X-ray spectra of FI and BI were simultaneously fitted with an absorbed power-law plus one broad line, $\text{Abs} \times (\text{Power-Law} + 1 \text{ Gaussian line})$, which is the same model as that of the XMM-Newton by Sidoli et al. (2006). The best-fit (90% confidence range) power-law index, line center energy, and width (1σ) are 1.2 (0.8–1.5), 6.66 (6.54–6.77) keV, and 0.31 (0.21–0.39) keV, respectively. These parameter values are the same as those of XMM-Newton within the statistical error. However, the Suzaku spectrum exhibits significant residuals near to energies of 6.4, 6.7 and 7.0 keV. We therefore fitted with a model of an absorbed power-law plus 3 narrow lines near to 6.40, 6.68 and 6.97 keV, $\text{Abs} \times (\text{Power-Law} + 3 \text{ Gaussian lines})$. Although the fittings were made simultaneously for the FI and BI spectra, we simply show the FI result in figure 3. The fit was largely improved using the energy of the line complex with χ^2/dof of 67.6/64. The best-fit parameters are listed in table 2.

The best-fit line energies of 6.7 keV and 7.0 keV are likely due to $K\alpha$ lines from He-like and H-like irons at energies of 6.68 keV and 6.97 keV, respectively, while the 6.4 keV line would be a $K\alpha$ line from neutral irons. The 6.97 keV line may be contaminated by a $K\beta$ line (7.05 keV) of

neutral irons. We therefore applied a more physical model: an absorbed thin thermal plasma (APEC) plus the 6.40 keV and 7.05 keV lines from neutral irons, $\text{Abs} \times (\text{APEC} + 6.40 \text{ keV} + 7.05 \text{ keV lines})$. In this model, we fixed the flux ratio of the 6.40 keV and 7.05 keV lines to 1: 0.125 (Kasstra & Mewe 1993). A simultaneous fit for the FI and BI spectra gave a nice fit with χ^2/dof of 77.4/65, as is given in table 2. In figure 4, we show the FI spectrum only for simplicity.

3.3. Timing

We examined a long-term (8 years) X-ray flux history from the 5 observations listed in table 1. The X-ray fluxes were calculated while fixing the same spectral shape given in table 2 of the 3-line model. The free parameter was only the normalization. The resultant fluxes in the 3–10 keV band show no significant variation during the 8 years interval. We then searched for a coherent pulsation from all of the observations listed in table 1. The Fast Fourier Transform (FFT) analysis revealed a clear peak at $\sim 1.7 \times 10^{-3}$ Hz from all of the observations. We then searched for accurate pulse period with the folding technique, and found a significant peak near to on the trial period of 593 sec. The best-fit pulse periods and errors are listed in table 3 for all of the observations. As an example, we show the Suzaku results from 2007: the power spectrum of FFT, folding result, and folded light curve in figure 5a, 5b, and 5c, respectively.

The 593-sec pulsation is likely to be a spin rotation of either a magnetic white dwarf or a neutron star in a binary system (see section 4). We, therefore, searched for an orbital modulation in the light curve with 1000-sec binning. In the Suzaku observations, we found no sign of orbital modulation, nor any sign of an eclipse. The time coverage of the XMM-Newton data was less than the Suzaku, and hence no orbital modulation was also found.

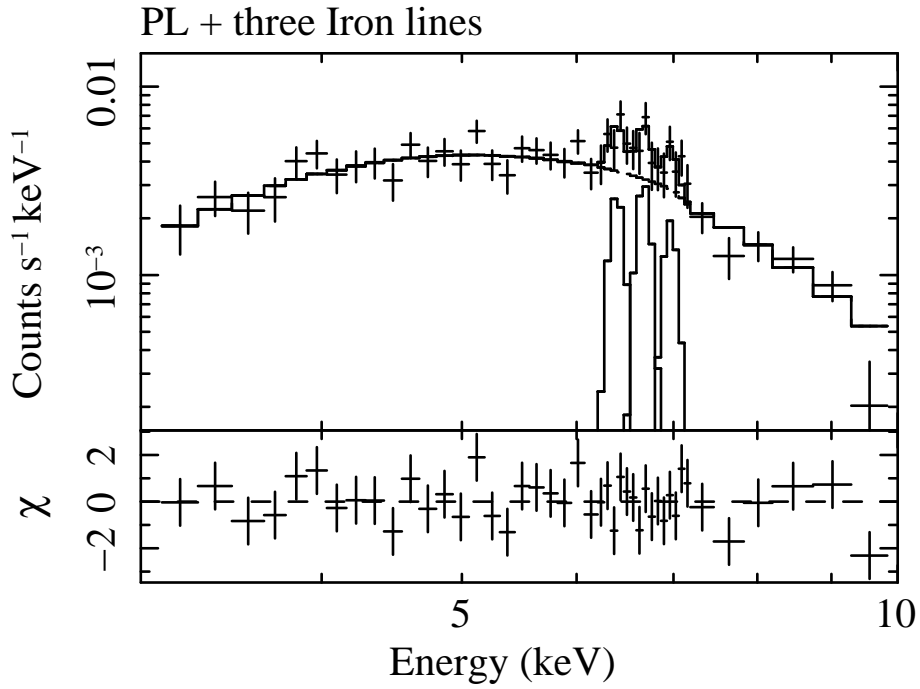


Fig. 3. Background-subtracted spectrum of SAX J1748.2–2808 for the FI CCD. The source spectrum was made from the solid polygons in figures 1a and 1b, while the local background spectra were taken from the dashed squares excluding the dashed ellipses. The solid line is the best-fit model of an absorbed power-law plus 3 Gaussians.

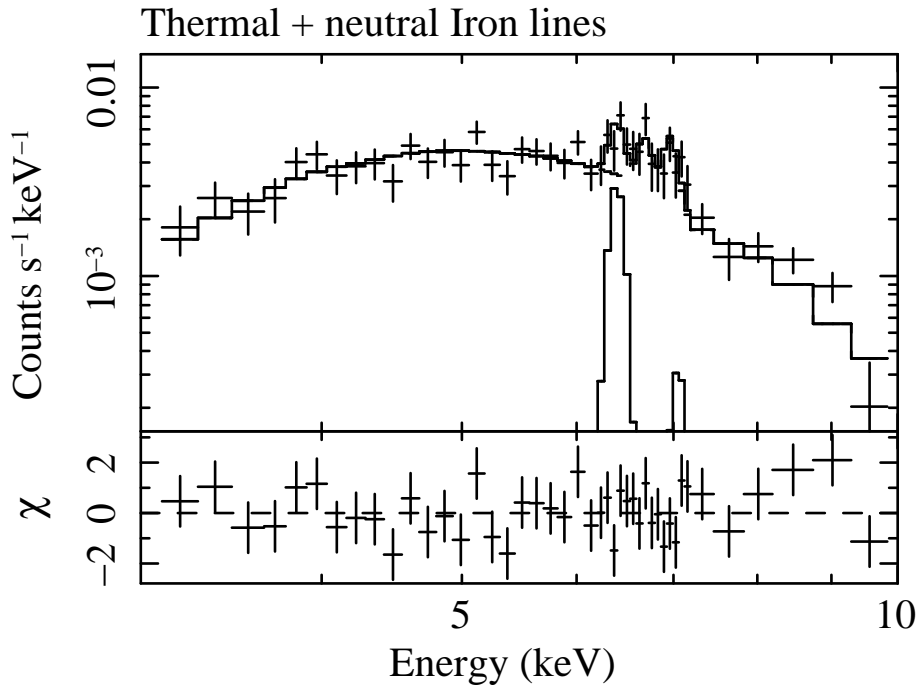


Fig. 4. Same as figure 3, but the best-fit model of an absorbed thin thermal plasma (APEC) plus K-shell lines of neutral iron.

Table 2. Best-fit parameters

Model: Abs×(Power-Law + 3 Gaussian Lines)		
Line Energy (keV)	Flux (10^{-6} ph s $^{-1}$ cm $^{-2}$)	Equivalent Width (eV)
6.40 (6.39–6.47)	1.5 (0.8–2.3)	140 (30–270)
6.68 (6.66–6.72)	1.9 (1.1–2.7)	180 (30–350)
6.97 (6.94–7.46)	1.3 (0.6–2.1)	130 (\leq 270)
Parameter	Best-Fit Value	
Power-Law Index	1.0 (0.8–1.3)	
N_{H} (10^{23} cm $^{-2}$)	1.3 (1.0–1.7)	
Flux (3–10 keV) (10^{-13} erg s $^{-1}$ cm $^{-2}$)	6.0 (5.7–6.2)	
Luminosity † (3–10 keV) (10^{33} erg s $^{-1}$)	7.4 (7.0–7.6)	
χ^2 / dof	67.6 / 64	
Model: Abs×(APEC + Neutral Iron Lines)		
Line Energy (keV)	Flux (10^{-6} ph s $^{-1}$ cm $^{-2}$)	Equivalent Width (eV)
6.40 ‡	2.1 (1.0–2.7)	160 (10–270)
7.05 ‡	0.26 ‡	—
Parameter	Best-Fit Value	
Temperature: kT (keV)	12 (9–17)	
Metal abundance (solar)	0.57 (0.35–0.85)	
N_{H} (10^{23} cm $^{-2}$)	1.8 (1.6–2.1)	
Flux (3–10 keV) (10^{-13} erg s $^{-1}$ cm $^{-2}$)	5.4 (5.2–5.7)	
Luminosity † (3–10 keV) (10^{33} erg s $^{-1}$)	8.4 (8.0–8.8)	
χ^2 / dof	77.4 / 65	

* Parenthesis is 90% error range

† Absorption corrected. Distance toward SAX J1748.2–2808 is assumed to be 8.5 kpc.

‡ The line energies are fixed, and the flux of the 7.05 keV line is constrained to be 0.125 of the 6.40 keV Line.

Table 3. Best-fit Period

Observatory (Year/Month)	Instruments	Pulse Period (s)
XMM-Newton (2000/09)	MOS1+2	592 \pm 8
XMM-Newton (2000/09)	PN	594 \pm 8
XMM-Newton (2003/03)	MOS1+2	593 \pm 2
XMM-Newton (2005/02)	MOS1+2	595 \pm 3
XMM-Newton (2005/02)	PN	593 \pm 2
Suzaku (2007/09)	XIS 0+1+3	593.1 \pm 0.4
Suzaku (2008/03)	XIS 0+1+3	592.8 \pm 0.4

* Error is 1- σ of the Gaussian of the folded result (e.g. figure 5b).

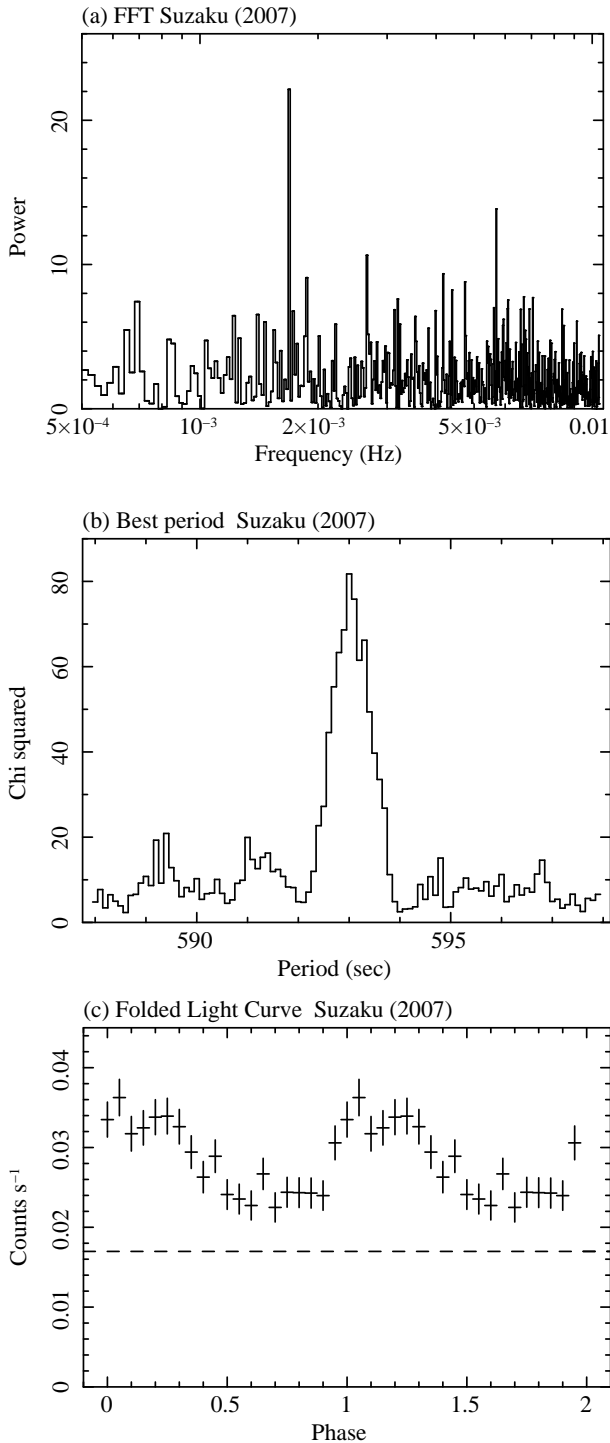


Fig. 5. (a): Power spectrum (FFT) of the Suzaku observation (2007). (b): Same as (a), but the folding results at around the trial period of 593 sec. (c): Same as (a), but the folded light curve at the best-fit period of 593.1 sec, where the dashed line is the background level.

4. Discussion

We found a coherent pulsation of 593-sec from SAX J1748.2–2808. This constrains the origin of this source to be either a magnetic CV, or a HMXB pulsar. The 593-sec period is among the slowest 10% of the pulse period in HMXB pulsars (Nagase et al. 1989, Liu et al. 2000), while the fastest 30% in magnetic CVs (Ritter et al. 2003). Thus, the spin period of 593-sec favors a magnetic CV scenario, although a HMXB pulsar scenario is not firmly excluded.

The Suzaku spectrum resolved the broad line at 6.6 keV found in the previous XMM-Newton observation into, at least, three lines at 6.40, 6.68, 6.97 keV. The best-fit equivalent width (EW) of these three lines are ~ 140 eV, ~ 180 eV, and ~ 130 eV, respectively. Ezuka and Ishida (1999) compiled the ASCA data and reported that the magnetic CVs exhibit 3 iron $K\alpha$ lines at 6.4, 6.7, and 7.0 keV with mean EW value of ~ 100 , ~ 200 , and ~ 100 eV, respectively (see also Hellier et al. 1998), nearly the same as those of SAX J1748.2–2808.

The overall spectrum was also well fitted with a thin thermal plasma of 12-keV temperature with a sub-solar iron abundance plus $K\alpha$ (6.40 keV) and $K\beta$ (7.05 keV) lines from neutral irons. Ezuka and Ishida (1999) also reported that the spectra of the magnetic CVs can be described by a thin thermal plasma model plus 6.4 keV line with a mean temperature of ~ 10 keV, closely resemble in the Suzaku results of SAX J1748.2–2808.

HMXB pulsars show a hard continuum spectrum, but it is a broken power-law and not a thin thermal. HMXBs exhibit an iron emission line feature. However, the line feature is not complex, but is a single line, mostly at 6.4 keV (see table 3 of Nagase et al. 1989). These properties are different from those of SAX J1748.2–2808.

All of the above facts favor the idea that SAX J1748.2–2808 is a magnetic CV rather than a HMXB. The pulse period of 593-sec is smaller than the possible orbital period, although we found no orbital modulation. Therefore, 593-sec would be the spin period, and hence SAX J1748.2–2808 is an intermediate polar (IP), not a polar with synchronized spin and an orbital period. A Typical IP has a luminosity of $\sim 10^{32}$ erg s^{-1} . If this luminosity is true for SAX J1748.2–2808, then from the observed flux of $\sim 6 \times 10^{-13}$ erg cm^{-2} s^{-1} , the distance is estimated to be ~ 1 kpc. Thus, SAX J1748.2–2808 would be a foreground source, not a member of the GC sources. Conversely, Sidoli et al. (2006) suspected that SAX J1748.2–2808 is located near the GC region at about 8.5 kpc, because it has a large absorption of 1.4×10^{23} H cm^{-2} . With this distance, they estimated the luminosity to be $\sim 10^{34}$ erg s^{-1} , significantly larger than any other magnetic CVs, and hence the authors declined to suggest a HMXB origin. We, however, note that a large fraction of the absorption of IPs is due to the circum-stellar gas. Therefore, the large absorption of SAX J1748.2–2808 would also be due to circum-stellar gas, rather than interstellar gas integrated along the long line of sight. This large amount of circum-stellar gas can

be naturally explained as being the origin of the strong 6.4 keV line from neutral irons (see e.g. Ezuka & Ishida 1999).

The authors thank all of the Suzaku team members, especially Y. Hyodo, H. Uchiyama, M. Ozawa, H. Nakajima, H. Yamaguchi, and H. Mori for their supports and useful information on the XIS performance. This work is supported by Grant-in-Aids from the Ministry of Education, Culture, Sports, Science and Technology (MEXT) of Japan, Scientific Research A (KK), and Grant-in-Aid for Young Scientists B (HM). HM is also supported by the Sumitomo Foundation, Grant for Basic Science Research Projects, 071251, 2007. MN is supported by JSPS Research Fellowship for Young Scientists.

References

- Ezuka, H. & Ishida, M. 1999, *ApJS*, 120, 277
Hellier, C., Mukai, K. & Osborne, J. P. 1998, *MNRAS*, 297, 526
Hyodo, Y., Tsujimoto, M., Hamaguchi, K., Koyama, K., Kitamoto, S., Maeda, Y., Tsuboi, Y., & Ezo, Y. 2008, *PASJ*, 60, S85
Kaastra, J. S., & Mewe, R. 1993, *A&AS*, 97, 443
Koyama, K., et al. 2007a, *PASJ*, 59, S23
Koyama, K., et al. 2007b, *PASJ*, 59, S245
Liu, Q. Z., van Paradijs, J., & van den Heuvel, E. P. J. 2000, *A&AS*, 147, 25
Mitsuda, K., et al. 2007, *PASJ*, 59, S1
Muno, M. P., et al. 2003, *ApJ*, 589, 225
Muno, M. P., et al. 2004, *ApJ*, 613, 326
Muno, M. P., Bauer, F. E. Bandyopadhyay, R. M., & Wang, Q. D. 2006, *ApJS*, 165, 173
Nagase, F. 1989, *PASJ*, 41, 1
Ritter, H. & Kolb, U. 2003, *A&A*, 404, 301
Serlemitsos, P., et al. 2007, *PASJ*, 59, S9
Sidoli, L., Mereghetti, S., Treves, A., Parmar, A. N., Turolla, R., & Favata, F. 2001, *A&A*, 372, 651
Sidoli, L., Mereghetti, S., Favata, F., Oosterbroek, T., & Parmar, A. N. 2006, *A&A*, 456, 287
Strüder, L., et al. 2001, *A&A*, 365, L18
Tawa, N., et al. 2008, *PASJ*, 60, S11
Turner, M. J. L., et al. 2001, *A&A*, 365, L27
Uchiyama, H., et al. in prep.